

RESEARCH ARTICLE

10.1002/2014JD022938

Key Points:

- Time-independent constant for water clarity can be used for humic lake modeling
- The surface temperature response to water clarity changes sign during overturn
- Freeze over probably occurs earlier if the lake water clarity decreases

Correspondence to:

J. J. Heiskanen,
jouni.heiskanen@helsinki.fi

Citation:

Heiskanen, J. J., et al. (2015), Effects of water clarity on lake stratification and lake-atmosphere heat exchange, *J. Geophys. Res. Atmos.*, 120, 7412–7428, doi:10.1002/2014JD022938.

Received 3 DEC 2014

Accepted 1 JUL 2015

Accepted article online 3 JUL 2015

Published online 7 AUG 2015

Effects of water clarity on lake stratification and lake-atmosphere heat exchange

Jouni J. Heiskanen¹, Ivan Mammarella¹, Anne Ojala^{2,3}, Victor Stepanenko⁴, Kukka-Maaria Erkkilä¹, Heli Miettinen⁵, Heidi Sandström¹, Werner Eugster⁶, Matti Leppäranta¹, Heikki Järvinen¹, Timo Vesala^{1,2}, and Annika Nordbo^{1,7}

¹Department of Physics, University of Helsinki, Helsinki, Finland, ²Department of Forest Sciences, University of Helsinki, Helsinki, Finland, ³Department of Environmental Sciences, University of Helsinki, Lahti, Finland, ⁴Research Computing Center, Moscow State University, Moscow, Russia, ⁵Department of Environmental Sciences, University of Helsinki, Helsinki, Finland, ⁶Department of Environmental Systems Science, ETH Zürich, Zürich, Switzerland, ⁷Affiliation when she worked with this publication

Abstract Recent progress of including lake subroutines in numerical weather prediction (NWP) models has led to more accurate forecasts. In lake models, one essential parameter is water clarity, parameterized via the light extinction coefficient, K_d , for which a global constant value is usually used. We used direct eddy covariance fluxes and basic meteorological measurements coupled with lake water temperature and clarity measurements from a boreal lake to estimate the performance of two lake models, LAKE and FLake. These models represent two 1-D modeling frameworks broadly used in NWP. The results show that the lake models are very sensitive to changes in K_d when it is lower than 0.5 m^{-1} . The progress of thermal stratification depended strongly on K_d . In dark-water simulations the mixed layer was shallower, longwave and turbulent heat losses higher, and therefore the average water column temperatures lower than in clear-water simulations. Thus, changes in water clarity can also affect the onset of ice cover. The more complex LAKE modeled the seasonal thermocline deepening, whereas it remained virtually constant during summer in the FLake model. Both models overestimated the surface water temperatures by about 1°C and latent heat flux by $>30\%$, but the variations in heat storage and sensible heat flux were adequately simulated. Our results suggest that, at least for humic lakes, a lake-specific, but not time-depending, constant value for K_d can be used and that a global mapping of K_d would be most beneficial in regions with relatively clear lakes, e.g., in lakes at high altitudes.

1. Introduction

Lakes impact regional weather [Rooney and Bornemann, 2013], and consequently, lake subroutines have recently been implemented in numerical weather prediction (NWP) models, leading to improved forecast skills [e.g., Balsamo et al., 2012]. Global data on lake coverage and depth are essential for lake subroutines, and relevant data sets have recently been created [Kourzeneva et al., 2012]. In the boreal and tundra zone the snow and ice thicknesses in winter are essential quantities for the lake-atmosphere interaction [Yang et al., 2013; Leppäranta, 2015], and in the absence of thick snow cover solar radiation penetrates into the water body [Lei et al., 2011]. Therefore, another essential external parameter in lake models is water clarity, which determines how the radiation is distributed in the water column. This in turn affects thermal stratification, surface temperature, and heat storage in a lake and therefore directly influences the lake-atmosphere interaction. However, for water clarity, global data are not yet available, and water clarity measurements are not systematic.

Water clarity is described in lake models as a diffuse light extinction coefficient (K_d) that describes how shortwave radiative energy is absorbed within the lake water body as a function of depth. This coefficient is an apparent optical property that depends on the properties of lake water and the illumination conditions. K_d is known to vary more between lakes than seasonally within one lake [Arst et al., 2008]; e.g., a low-clarity lake (high K_d) acts similarly to a shallow lake since solar radiation is absorbed and immediately stored into the top layer of thickness $\sim K_d^{-1}$. The epilimnion (the upper layer) is thus shallower than in a clear-water lake, and the surface temperature is higher in spring and lower in autumn when cool water from the hypolimnion (the lower layer) is mixed into the epilimnion [Persson and Jones, 2008]. The higher spring surface temperatures lead to an increased heat loss via turbulent fluxes of sensible and latent heat in addition to larger longwave radiative cooling [Persson and Jones, 2008].

Water clarity is related to the amount of suspended particles and to the color of the water which is mainly the result of colored dissolved organic matter (CDOM) concentration—high concentration of CDOM has been shown to be tightly linked to low water clarity [Fee *et al.*, 1996; Pace and Cole, 2002; Arst *et al.*, 2008]. CDOM is connected to dissolved organic carbon (DOC), and colored DOC in the lake originates mainly from the watershed, whereas colorless DOC can result from excretion of the lake biota [Findlay and Sinsabaugh, 2003]. Some of the DOC can also originate in the littoral zone (shallow area near shore) and then be laterally transported to the pelagial (open-water zone). Heavy rain events often result in increased DOC loading from the watershed [Ojala *et al.*, 2011], and therefore, long-term atmospheric phenomena which affect precipitation patterns can substantially impact water clarity [Gaiser *et al.*, 2009]. The environmental factors (e.g., turbulence [Ji, 2008]) which affect the sedimentation rate of suspended particles such as algae can affect the visibility (the optical thickness) of the water as well as the yearly succession of plankton species [Jeppesen *et al.*, 1999]. Jeppesen *et al.* [1999] noticed that increase in phytoplankton concentrations lead to lower water clarity but that zooplankton has the opposite effect via grazing on phytoplankton.

Fee *et al.* [1996] observed a relatively strong link between low visibility and high chlorophyll *a* (Chl *a*) concentrations which is a measure of algal biomass. The impact of algal biomass to the thermal stratification of lakes has been studied using both enclosures [Jones *et al.*, 2005] and models [Rinke *et al.*, 2010]. Both studies concluded that the plankton biomass can affect thermal stratification if the biomass is high or the water is clear. The effect of long-term eutrophication on the water clarity has been demonstrated in a Finnish study of over 30 years where the increasing Chl *a* concentrations cooccurred with decreasing water clarity [Ventelä *et al.*, 2007].

Other factors affecting water clarity are inflow and outflow of suspended matter and, in shallow lakes, resuspension of bottom sediments [Arst *et al.*, 2008; Niemistö, 2008]; the effect of which is enhanced if upwelling of near-bottom waters to the surface occurs [Weyhenmeyer, 1998]. Thus, connections between terrestrial and aquatic ecosystems and hydrodynamics of lakes are of crucial importance for water clarity.

Water clarity is expected to influence mixed-layer depth of small lakes more than of large lakes since in small lakes the wind and wave-driven turbulent mixing is weaker due to shorter fetch and lower wind speed. Some studies show that water clarity affects the mixed layer depth only on small lakes [Fee *et al.*, 1996], whereas others show that even in the biggest lakes water clarity cannot be neglected [Thiery *et al.*, 2014b]. In clear water, light can penetrate deep into the water column resulting in a higher amount of energy stored into the lake as opposed to dark water which leads to a stronger thermocline (the layer between epilimnion and hypolimnion with the largest temperature gradient), shallower mixed layer, higher surface water temperatures, and thus higher heat loss [Hocking and Straškraba, 1999]. The sensitivity of mixed layer models to the water clarity was examined in the 1970s [see Niiler and Kraus, 1977]. More recently, this problem has been revisited for the sensitivity of lake models to K_d or DOC [e.g., Perroud and Goyette, 2010; Potes *et al.*, 2012; Read and Rose, 2013; Rooney and Bornemann, 2013]. These studies tested the sensitivity of the chosen model to water clarity with two clarity values, but none of these studies had direct flux measurements for the validation of simulation results.

According to the modeling results, global warming will lead to higher water temperatures in small lakes [Kirillin, 2010]. In addition to the relation to surface temperature and heat budgets, water clarity affects greenhouse gas budgets due to the effect of heat flux on gas transfer [Heiskanen *et al.*, 2014]. Small lakes are hot spots of biogeochemical cycling due to many factors, such as high biological activity and high surface water CO₂ and DOC concentrations [Cole *et al.*, 2007; Tranvik *et al.*, 2009; Downing, 2010]. The carbon cycle is influenced by the thermal cycle of lakes [White *et al.*, 2012]. For example, methane (CH₄) fluxes to the atmosphere can be expected to increase if the heat flux into the lake increases bottom temperature [Wik *et al.*, 2014], since higher sediment temperatures enhance the production rate of CH₄ [Schulz *et al.*, 1997]. Stronger stratification in turn increases the oxygen depletion in near-bottom waters which further enhances CH₄ production and dramatically reduces its oxidation.

The aim of this work is to assess how seasonal changes as well as the general level of K_d affect thermal stratification of small, humic lakes and how sensitive lake-atmosphere heat exchange is to K_d . We modeled water temperature profiles and turbulent fluxes of heat and momentum with two widely used one-dimensional lake models and compared the results to those measured with a thermistor chain and an

eddy covariance (EC) system from a small boreal lake during the ice-free period of 2013. According to our results, an increase in K_d leads to higher surface water temperature during summer and colder after the onset of autumn overturn, whereas a decrease in K_d has the opposite effect to surface temperature. This could lead to earlier freeze over if the lake becomes more turbid. According to the sensitivity analysis, a global database of at least clear-water lakes should be created and put to use in numerical weather prediction. In humic lakes with high K_d ($>0.5 \text{ m}^{-1}$) and where K_d is dominated by CDOM, the seasonal variation of K_d is small enough to allow the use of a constant value in time. This study is the first to assess model sensitivity to K_d using direct EC flux measurements.

2. Methods

2.1. Lake Models

The chosen models are (1) the multilayer model LAKE [Stepanenko *et al.*, 2011] and (2) the self-similarity concept-based model FLake [Mironov *et al.*, 2010; Kirillin *et al.*, 2011] which assumes a parameterized temperature profile. The water column in FLake is divided into a mixed layer where temperature is constant and a thermocline which is parameterized as fourth-order polynomial and can thus vary from isothermal to a sharp temperature curve. Treating the temperature profile in a self-similar form allows the heat conduction to be solved from ordinary differential equations which enables high computational efficiency. This has led to its recent implementation into several land surface schemes of NWP models: the Consortium for Small-Scale Modeling model [Mironov *et al.*, 2010], the High-Resolution Limited-Area Model [Eerola *et al.*, 2010; Rontu *et al.*, 2012], the Surfex model [Salgado and Le Moigne, 2010], the model of the United Kingdom Met Office Unified Model [Rooney and Jones, 2010], and the H-TESSSEL land surface scheme of Integrated Forecasting System developed in the European Centre for Medium-Range Weather Forecast [Dutra *et al.*, 2010; Balsamo *et al.*, 2012].

The LAKE model treats the water column as multiple layers (20 in this study), and it is thus computationally more expensive than the FLake model [Thiery *et al.*, 2014a] but predicts water temperature more accurately. The model solves five core prognostic equations: horizontal momentum components, heat conduction, turbulent kinetic energy (TKE, k), and rate of TKE dissipation (ϵ). Turbulent diffusivity and eddy viscosity are accordingly calculated using a k - ϵ closure scheme and thus are treated as shear and stability dependent. Momentum flux at the surface is partially consumed in wave development and the remainder used to drive currents [Stepanenko *et al.*, 2014]. The bottom sediments are treated with multiple layers (here 10), and interaction with the water column is solved. The model also contains subroutines for ice and snow processes, but they are not relevant in this study and thus will not be further discussed. Recent lake model intercomparison studies [Stepanenko *et al.*, 2013, 2014] have shown that LAKE model performance is very close to that of other k - ϵ models in terms of surface heat balance and in-lake temperature profiles. Therefore, this model may be regarded as a good representative of k - ϵ models in general.

Aerodynamic roughness length, z_0 (m), is an important parameter in lake models since it influences the drag coefficient and the Stanton and Dalton numbers which, in turn, are used for parameterizing the fluxes of momentum, sensible, and latent heat, respectively.

The meteorological forcing variables of the models are air temperature (T_a), wind speed (U), specific humidity (q), incoming shortwave ($SW\downarrow$) and longwave radiation ($LW\downarrow$), and air pressure (p). LAKE additionally uses wind direction and precipitation. Water inflows and outflows are dynamically adjusted to keep the lake water level nearly constant. The models simulate the water temperature profile independently, but surface flux parameterizations in both models are from FLake. Surface fluxes of momentum, heat, and water vapor are solved according to Monin-Obukhov similarity theory, and the roughness length is dependent on a normalized fetch to take into account the distance from the shore. Incoming solar radiation is reflected with a constant albedo. In LAKE the near-infrared fraction of shortwave radiation (35% of $SW\downarrow$) is immediately absorbed at the surface, while the remaining part is transferred to the deeper layers. In both models, the energy penetrating below the surface attenuates in the water according to Beer-Lambert's law. In FLake, this attenuation can be treated separately for eight wavelength bands (not used here). Although we assumed in FLake that K_d is equal for all $SW\downarrow$ wavelengths, this probably has little influence on the results since in humic Lake Kuivajärvi, with an average thermocline depth of 5 m, over 95% of $SW\downarrow$ is absorbed in the mixed layer. LAKE includes an option for including lake morphometry via the

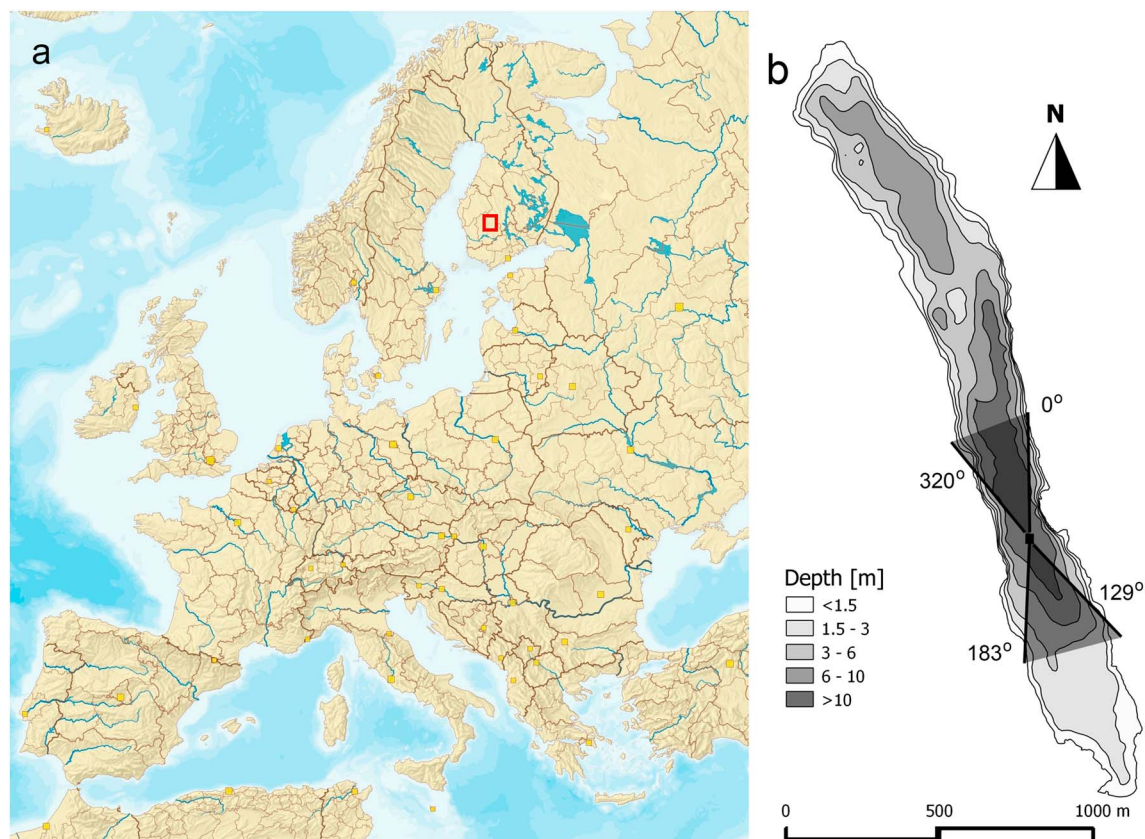


Figure 1. (a) The location of Lake Kuivajärvi in Europe (red square, map the courtesy of Atlas of Switzerland 3.0, reproduced with the permission from Swisstopo (JD100042)). (b) The bathymetry of Lake Kuivajärvi with the measurement raft (black square) and wind directions of acceptable EC data (dark patches). The patch length corresponds to the median fetch (410 m).

hypsothetic curve, but this option was not used in our simulations since it has been shown to cause excessive warming in deep waters if not accounting for lateral heat exchange between the water body and the bottom [Stepanenko *et al.*, 2014]. The cool skin parameterization in LAKE [Chechin *et al.*, 2010] was switched off to make the models more consistent in this respect, since there is no such parameterization in FLake.

2.2. Measurement Site and Data Acquisition

Lake Kuivajärvi is a small (area 0.62 km², mean depth 6.4 m) mesotrophic, dimictic lake in Finland (24°16'E, 61°50'N; 141 m above sea level) next to the well-established SMEAR II forest site (Station for Measuring Ecosystem-Atmosphere Relations) [Hari and Kulmala, 2005]. The catchment area is 9.4 km² of mostly flat terrain having primarily a Haplic Podzol soil type covered by mostly managed pine forest [Miettinen *et al.*, 2015]. The lake is elongated with a maximum length of 2.6 km and a modal fetch of 410 m (Figure 1). The lake has two main basins, the larger and deeper having maximum depth of 13.2 m [Heiskanen *et al.*, 2014]. The Secchi depth has been routinely measured in the lake since 2009 (typically weekly measurements around noon during the open-water season), and it ranges from 1.2 to 1.5 m. Secchi depth is a fast and easy manual method to visually estimate the water clarity with a submerged white plate. The lake is typically frozen for about 5 months during a year. After ice out, turnover of the water mass occurs immediately and a thermocline starts developing. The thermocline deepens until the autumn turnover occurs, and thereafter, the lake freezes over again [Miettinen *et al.*, 2015]. The maximum heat content is typically reached in August.

Measurements on the lake have been ongoing since 2009. For this study we selected the open-water period of 2013. A measurement raft is moored at the center of the deeper basin where the depth is 12 m. The suite of instruments included an EC flux measurement array consisting of an ultrasonic anemometer (USA-1, Metek GmbH, Germany) and an enclosed-path infrared gas analyzer (LI-7200, LI-COR Inc., Nebraska, USA). The

Table 1. Model Forcing Atmospheric Variables and Relevant Information

Variable	Height (m)	Sensor (Manufacturer)	Nominal Accuracy	Gap-Filled Data (%)	Backup Data (Sensor) [RMSE]
Air temperature (T_a , K)	1.7 ^a	Ultrasonic anemometer USA-1 (Metek)	0.01 K	28	SMEAR II, 4.2 m, Pt-100 [0.7 K]
Wind speed (U , m s^{-1})	1.7	Ultrasonic anemometer USA-1 (Metek)	0.01 m s^{-1}	9	SMEAR II, 16.8 m USA-1 [0.9 m s^{-1}]
Specific humidity (q , kg kg^{-1}) ^b	1.5	RH from Rotronic sensor (Rotronic Instrument Corp.)	0.8% RH	34	SMEAR II, 16.8 m RH (Rotronic Hygromet MP102H with Hygroclip HC2-S3, Rotronic AG, Bassersdorf, Switzerland) [0.6 g kg^{-1}]
Incoming shortwave radiation ($\text{SW}\downarrow$, W m^{-2})	1.5	CM3 on CNR-1 net radiometer (Kipp & Zonen B.V.)	3.4 W m^{-2}	4	SMEAR II, Middleton Solar SK08 First Class Pyranometer (Middleton Solar, Yarraville, Australia) [28 W m^{-2}]
Incoming longwave radiation ($\text{LW}\downarrow$, W m^{-2})	1.5	CG3 on CNR-1 net radiometer (Kipp & Zonen B.V.)	3.4 W m^{-2}	4	SMEAR II, 33.0 m CNR1 net radiometer (Kipp & Zonen, Delft, Netherlands) [14 W m^{-2}]
Air pressure (p , Pa)	1.5	DPI260 barometer (General Eastern Instruments, Woburn, MA, USA)	50 Pa	0	-
Precipitation (mm h^{-1}) ^c	18	FD12P Weather sensor, Precipitation and visibility meter (Vaisala Oyj, Helsinki, Finland)	-	0	-

^aHeight changed from 1.7 to 1.5 using Businger-Dyer formulations in the flux-gradient relationship. Effect was 0.32%.

^bCalculated from relative humidity (RH), air temperature, and pressure.

^cAt SMEAR II, above forest at 18 m height.

length of the PTFE sampling tube was 3.5 m, the inside diameter 4 mm, and the flow rate 8 L m^{-1} . The EC setup allows measurements of the sensible heat (H) and latent heat (LE) fluxes and momentum flux (τ). On the raft, a four-way net radiometer (CNR-1) provided the full radiation budget (shortwave and longwave), and a thermistor string of 16 Pt-100 resistance thermometers (accuracy 0.2°C ; depths 0.2, 0.5, 1.0, 1.5, 2.0, 2.5, 3.0, 3.5, 4.0, 4.5, 5.0, 6.0, 7.0, 8.0, 10.0, and 12.0 m) enabled the calculation of the heat storage in water and the thermocline depth according to *Nordbo et al.* [2011]. All the atmospheric measurements were performed at a height of 1.7 m above the water, and 30 min averages were calculated for the analyses. In addition, the relative humidity (RH) was directly measured at the raft at a height of 1.5 m (MP102H-530300, Rotronic AG, Switzerland). Fast measurements of the platform tilt angles were conducted with a dual-axis inclinometer, but the tilting correction is unnecessary for Lake Kuivajärvi [*Mammarella et al.*, 2015]. Model forcing variables and the corresponding instrumentation are given in Table 1. For more information on the measurement setup, see *Heiskanen et al.* [2014] and *Mammarella et al.* [2015].

Turbulent fluxes of sensible and latent heat and momentum were calculated from 10 Hz raw data using standard procedures implemented in EddyUH, a versatile software for EC flux calculations, developed at the University of Helsinki (www.atm.helsinki.fi/Eddy_Covariance/EddyUHsoftware.php). Raw data were despiked [*Vickers and Mahrt*, 1997a], a two-dimensional coordinate rotation [*Kaimal and Finnigan*, 1994] was applied, cross-wind correction was done to sonic temperature data [*Liu et al.*, 2001], and the mixing ratio of water vapor was converted relative to dry air before the calculation of covariances. The maximum of the cross-covariance function was used for defining the lag time between the water vapor signal relative to the vertical wind speed. A linear trend was removed from the cross-covariance function [*Clement*, 2004], and the lag time was allowed to depend on RH [*Nordbo et al.*, 2012]. Covariances were corrected for loss due to high- and low-frequency attenuation according to *Mammarella et al.* [2009], where the high-frequency correction of water vapor depended on RH.

The EC fluxes were checked for quality according to the steady state test and integral turbulence characteristics [*Foken and Wichura*, 1996]. Data with overall quality flag less than 4 were used. In addition, flux data were omitted when the wind direction (WD) was not along the lake ($0^\circ < \text{WD} < 129^\circ$, $183^\circ < \text{WD} < 320^\circ$; Figure 1) since under these conditions the flux source area (i.e., footprint) extends into the lake shoreline. Due to wind direction, 24% of the 30 min data records were omitted. Other factors resulted in there being 51%, 39%, and 35% of data left for H , LE , and momentum fluxes, respectively. The site has an energy balance closure of 80% [*Mammarella et al.*, 2015].

In addition to basic meteorology and turbulent fluxes, we made continuous measurements of K_{dPAR} for the photosynthetically active radiation (PAR; 400–700 nm) as well as campaign-wise spectral measurements. Irradiance in water (I_w) decays according to the Beer-Lambert law as a function of depth (z ; m):

$$I_w(z) = I_0 \exp(-K_{dPAR}z), \quad (1)$$

where I_0 is the PAR irradiance just beneath the surface. In reality, K_d depends on wavelength, the optically active substances in the water and illumination conditions (i.e., solar zenith angle, cloudiness, and angular distribution of radiation). K_{dPAR} depends on the spectral distributions of K_d , and I can be converted to percent transmission per meter, T_{1m} (estimated here as $T_{1m} = 100 \exp(-K_d * 1 \text{ m})$), which gives the relative amount of radiation left at the depth of 1 m.

For continuous monitoring, PAR irradiance was measured at the depth of 0.2 m in the lake (LI-192, LI-COR Inc., Nebraska, USA), and incoming PAR (I_a) was available at the forest station 750 m away from the measurement raft (LI-190SZ, LI-COR Inc., Nebraska, USA). The value of K_{dPAR} was calculated as

$$K_{dPAR} = -\frac{\ln\left(\frac{I_w}{I_0}\right)}{\frac{\Delta z}{\cos(\theta)}}, \quad (2)$$

where I_0 is the part of I_a that was not reflected off the surface (i.e., $I_0 = (1 - a)I_a$, a is the albedo of PAR at the lake) and Δz is the measurement depth of aquatic PAR (0.2 m), which is corrected for the representative solar zenith angle, θ . Note that the zenith angle is not exactly representative for radiance paths for irradiance since cloudiness and surface roughness affect radiance paths. The PAR range is taken to be sufficient in equation (2) because the contribution of wavelengths outside PAR to the thermal energy of the water column is at a level of a few percent below the near-surface layer [Kirk, 2011].

For the campaign, a spectroradiometer (RAMSES, TriOS Optical Sensors, Germany) was used. It measures the spectral irradiance for 3.3 nm wavelength bands between 320 and 950 nm resulting in 190 measurements per scan. Measurements were made on 18 June 2014 and 23 July 2014 (a year later than the data used for simulations). The measurement depths were 0.02, 0.05, 0.10, 0.15, 0.20, 0.30, 0.50, 0.75, 1.0, 1.5, and 2.0 m. For the determination of K_d , an exponential fit (equation (1)) was made from the surface to each depth point so that at least the first four depths were included, and the fit with the smallest root-mean-square error (RMSE) was chosen as the best.

For determining DOC (samples from 0.2 m depth) and Chl a (samples from 0–3 m) concentrations, weekly water samples were taken with a Limnos® water sampler (volume 2.0 L). From these, DOC and Chl a were determined as in Ojala *et al.* [2011].

2.3. Thermal Cycle and Simulation Setup

In 2013, ice-out took place on 1 May. Spring turnover followed immediately, and the surface temperature (T_s) was 3.4°C. The autumn turnover took place on 11 October when T_s had cooled down to 4.6°C. The lake froze over on 24 November. The simulation was started when the lake was isothermal, using the measured water column average temperature of 3.6°C in spring and ran until the end of October.

A standard simulation was performed with a seasonally averaged, measured K_{dPAR} ($=0.59 \text{ m}^{-1}$), a constant fetch of 410 m (median value of footprint calculations), lake depth of 12 m (depth at the measurement site), emissivity of 0.99, and a constant albedo of 0.07. In Lake Kuivajärvi, albedo varies between 0.05 and 0.1 during open-water period, and therefore, we assume that using a constant value produces only minor error in the modeling. Interactions with the bottom sediments were included. We used a spin-up time of 4 weeks, and validation data were omitted for this period. An additional set of 20 runs was made with selected K_d values that remained constant throughout the simulation period.

2.4. Driver Variables and Gap Filling

Forcing variables of air temperature, wind speed, humidity, and incoming shortwave and longwave radiation were measured directly on the lake. Pressure was measured at the forest site 750 m away from the raft. The longest measurement break during the open-water period 2013 was in the end of June (Figure 2). Backup data for all of the forcing variables were available at the forest site (the base of the mast being about 750 m away and 40 m higher than the raft), and the instrumentation is given in Table 1. Gap

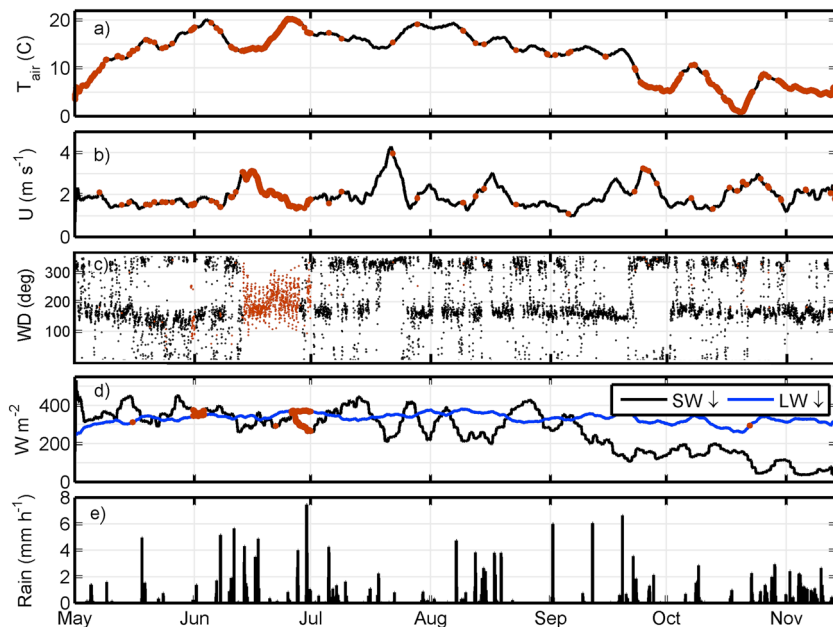


Figure 2. Forcing time series from Lake Kuivajärvi in 2013. (a) Air temperature ($^{\circ}\text{C}$), (b) wind speed (m s^{-1}), (c) wind direction (degree), (d) incoming shortwave (black line) and longwave (blue line) radiation (W m^{-2}), and (e) precipitation (mm h^{-1}). Values are 5 day running means of 30 min data (except for wind direction and rain), and only daytime values for incoming shortwave radiation are used. Gap-filled data are shown in brown.

filling was performed using monthly linear fits, and the percent of gap-filled data and the RMSE between above-lake and forest measurements are also given in Table 1. The forcing time series of the light extinction coefficient was made using data only when the solar zenith angle was below 75° to avoid problems with low solar angles. A 21 day running median was calculated to reduce scatter and to gap fill the K_d data.

3. Results and Discussion

3.1. Atmospheric Forcing

The 5 day running means of the gap-filled atmospheric forcing during the open-water period 2013 are presented in Figure 2. Air temperature was 4.5°C in the beginning, rising to the highest value, 20.4°C , in the end of June, until gradually declining to approximately 5°C in November (Figure 2a). The average wind speed was 2 m s^{-1} , and a windy period was observed in mid-July (Figure 2b), when 5 day wind speeds exceeded 4 m s^{-1} . Winds were typically blowing along the lake, either from north or from south, as is typical of Lake Kuivajärvi (Figure 2c). Incoming shortwave radiation had a declining trend from around 400 W m^{-2} in the beginning of the measurements to around 100 W m^{-2} in the end, whereas incoming longwave radiation was around 320 W m^{-2} during the whole study (Figure 2d). The median albedo was 0.07 (0.01 resolution, not shown) during the study period. The rain intensities were in general low, $<4 \text{ mm h}^{-1}$ almost all the time, although there were periods with rain almost every day for about 2 weeks, as seen in mid-June, August, and in the beginning of November (Figure 2e).

3.2. Roughness Parameterization

The roughness length calculated from EC measurements was much higher than in the original parameterization for oceans: the Charnock parameter α was 0.38 instead of the original 0.015 (Figure 3). The higher observed turbulent fluxes than expected with the given wind speed points to other sources contributing to TKE in addition to surface layer wind shear. This additional source was probably the transported large eddies from the surrounding forest with rougher surface conditions [Vesala *et al.*, 2012]. Therefore, using the roughness parameter calculated from observations forces the lake models to calculate the same momentum and turbulent heat fluxes as measured with the EC.

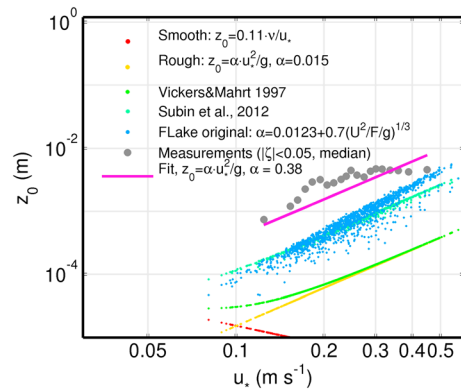


Figure 3. Roughness length (z_0 , m) as a function of friction velocity (u_* , m s^{-1}). The parameterizations by Charnock [1955] for smooth and rough flows (ν is the kinematic viscosity of air), by Vickers and Mahrt [1997b] and Subin et al. [2012], and the original parameterization in the FLake model (U is the wind speed, F is the fetch, and g is the gravitational acceleration) are shown. The measurements during near-neutral conditions (Obukhov stability parameter values $|\zeta| < 0.05$) are also shown as median bins, as well as a Charnock equation for rough flow with the increased Charnock parameter, $\alpha = 0.38$.

It has been demonstrated that the roughness of lakes exposed to weak winds is higher than that of an ocean [Wüest and Lorke, 2003]. The measured values were also higher than predicted by a parameterization for lakes [Subin et al., 2012] and the parameterization in the FLake model used here. The FLake model takes into account the dependency of α on fetch and wind speed, but clearly, this parameterization does not work for a small sheltered lake. Stepanenko et al. [2014] observed that the roughness is a crucial parameter for correct simulation of mixed layer depth in a lake. Thus, in this study, we used $\alpha = 0.38$ in the flux parameterizations of both models.

3.3. Observed Water Clarity

There was large scatter in K_d derived from the measurements (equation (2)), which was expected since the fluctuation in underwater irradiance is high on short time scales [Hieronymi and Macke, 2012]. The median value for K_d was 0.59 m^{-1} (25th percentile 0.43 and 75th percentile 0.79 ; Figure 4a). K_d was lowest during both spring and autumn overturns, $\sim 0.5 \text{ m}^{-1}$, and highest midsummer, $\sim 0.7 \text{ m}^{-1}$. DOC was highest in spring, almost 15 mg L^{-1} (Figure 4b), and declined then concomitantly with the progress of stratification. DOC

reached the lowest values just before autumn overturn, $< 11 \text{ mg L}^{-1}$, after which a slow increase followed. The 2013 chlorophyll data were not available, but according to 2011–2012 data (not shown), after ice-off Chl *a* rises from $< 10 \mu\text{g L}^{-1}$ to $30\text{--}50 \mu\text{g L}^{-1}$ in mid-July and then declines to $< 2 \mu\text{g L}^{-1}$ in late autumn.

Williamson et al. [1996] noted that when DOC concentrations were high in general, the seasonal variation in DOC hardly affects K_d , which probably was the case in Lake Kuivajärvi with high DOC concentrations. The data suggest that DOC defined the general level of K_d , whereas the yearly succession of plankton may explain the small but visible intraannual pattern in K_d . We lacked the data of particulate matter concentration, but expected it to be low since there are no shallow areas near the measurement site, and during summer the inflow from streams is low.

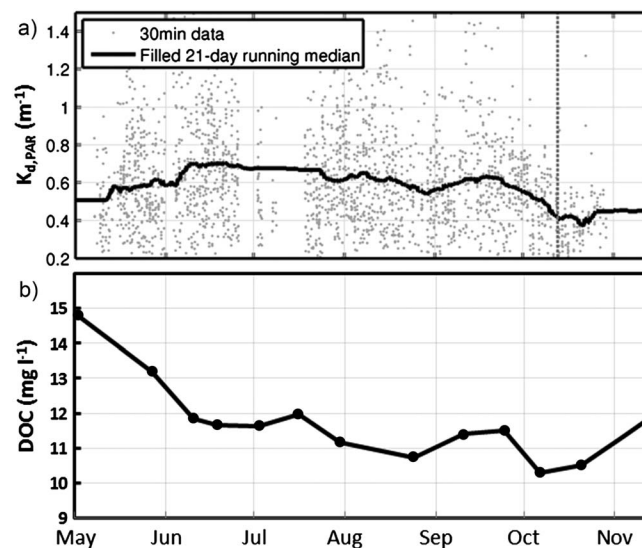


Figure 4. Time series of (a) diffuse light extinction coefficient ($K_{d,PAR}$, m^{-1}) for the PAR (400–700 nm) in Lake Kuivajärvi (the onset of turnover is marked with vertical dashed line) and (b) DOC concentration (mg L^{-1}) in 2013.

The relation of DOC concentration and water clarity is often estimated from regression curves based on a collection of different lakes [Morris et al., 1995; Rae et al., 2001; Read and Rose, 2013]. These show a wide range of variation in K_d from 0.3 to 5 m^{-1} , in the DOC concentration range of our study, $0.8\text{--}1.2 \text{ mmol L}^{-1}$. This makes sense since lakes are optically complex water bodies where the optical properties depend not only on DOC (more specifically colored dissolved organic matter) but also on suspended matter and Chl *a*. The measured Secchi depth from Lake Kuivajärvi and the regression equation by Arst et al. [2008] to estimate K_d would yield a value of

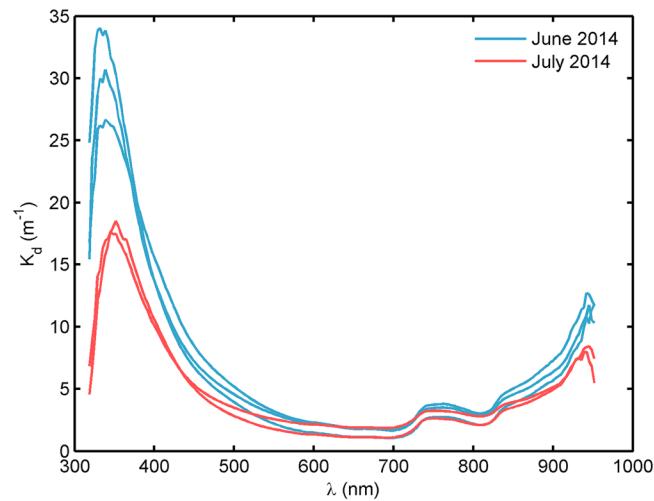


Figure 5. Diffuse light extinction coefficient (K_d , m^{-1}) as a function of wavelength (λ , nm) for June 2014 (three measurements per day) and July 2014 (two measurements, similarly).

about 1.3 m^{-1} . However, also in *Arst et al.* [2008], the scatter of K_d between lakes was high with Secchi depths similar to that of Lake Kuivajärvi (K_d ranging from $<1.0 \text{ m}^{-1}$ to about 4 m^{-1}), which suggests that the estimation of K_d from Secchi depth should be used with caution. Since DOC quality affects K_d , and the attenuation coefficients differ for different wavelengths [Morris et al., 1995], comparison between different lakes is difficult if not made within the same region with similar DOC composition, and indeed, Lake Kuivajärvi has similar K_d as some other lakes in the same region with similar DOC and Chl *a* concentrations [Arst et al., 1997].

The spectral dependency of K_d showed that blue wavelengths (due to colored dissolved organic matter) and near-infrared wavelengths (due to pure water) are strongly attenuated. Radiation with a wavelength of about 700 nm was attenuated the least (Figure 5). This observation is very common for similar type lakes in Finland and Estonia [Arst et al., 2008, their Figure 10]. Short wavelengths were attenuated more in June than in July which can be attributed to the amount of organic carbon and Chl *a*. The attenuation of different wavelengths depends also on solar zenith angle during sunny days [Zheng et al., 2002] and cloudiness. This should not have a significant impact on K_d in Lake Kuivajärvi, since most days in Finland are at least partially cloudy and the shown variation of K_d (on the order of 0.1 m^{-1}) according to solar zenith angle was only related to red wavelengths.

3.4. Water Temperature Profile and Energy Fluxes

In Lake Kuivajärvi the thermocline developed at about 2 m depth in the spring and deepened to 9 m before the autumn turnover in October (Figure 6a). In FLake simulations, the surface water temperature was on average 1.1°C too high, more so in autumn (Figure 6b), the mixing too strong, and the thermocline depth erroneously remained nearly constant. Contrastingly, the LAKE model simulated the thermocline deepening correctly, but the surface was also too warm (1.0°C), and the temperature fell too fast as a function of depth (Figure 6c), perhaps indicating some missing mixing mechanisms in the thermocline, e.g., gravity waves breaking, Kelvin-Helmholtz instabilities, or seiching. Note that the models did not use cool skin parameterization and the modeled T_s are compared to the measured T_s at 20 cm depth. Especially in turbulent conditions we expect this to be a minor source of error.

The partitioning of surface momentum flux into wave development and surface water shear stress prevented too deep mixing. LAKE was able to simulate the temperature stratification better than FLake, indicating that the multilayer approach is better suited than a parametric representation. An overestimation of $0.1\text{--}1.1^\circ\text{C}$ in the surface water temperature was also seen in five models for Lake Valkea-Kotinen (Finland, 0.014 km^2 [Stepanenko et al., 2014]). In the same study, it was concluded that the constant thermocline depth in FLake was caused by an insufficient mixed-layer development when winds were weak, as is the case for this small sheltered lake, too.

From the beginning of the study period to mid-August, up to 392 MJ m^{-2} of heat were stored in the water body. This energy was released back to the atmosphere by the end of the study period. While the heat content in the end of the period was actually 2 MJ m^{-2} lower than in the beginning, this value is within experimental uncertainty and hence close to the expected zero difference over the course of a full open-water period under the assumption of steady state conditions. Both models were able to simulate the total heat storage at the mid-August peak very closely (FLake 384 MJ m^{-2} and LAKE 377 MJ m^{-2}), but LAKE

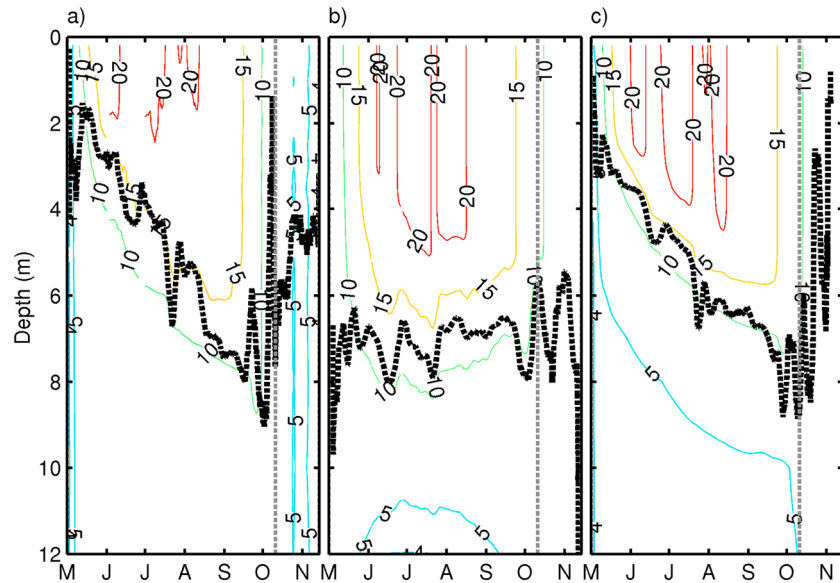


Figure 6. Water temperature ($^{\circ}\text{C}$) profile as a function of time: (a) measured, (b) modeled with FLake, and (c) modeled with LAKE. Temperature is given on contours, the thermocline is shown with a black dashed line, and the turnover period is shown with a gray dashed line. The data are 5 day running means.

simulated too much heat in the water body at the end of the period (72 MJ m^{-2}), whereas FLake simulated a net loss of heat (-18 MJ m^{-2}).

The sensible heat flux was simulated well by FLake (coefficient of determination, $r^2 = 0.80$, slope of the linear fit 0.75, and the y intercept 6.43) and LAKE ($r^2 = 0.83$, slope = 0.79, and y intercept = 3.12), although both failed in simulating the extreme values of H (Figures 7a and 7d). The simulated diel variations of H followed the measurements, and the seasonal and diel variation in the heat storage change was successfully described by both models (Figure 8). Latent heat flux was consistently overestimated by both models (FLake by 34% on average, $r^2 = 0.69$; LAKE by 35%, $r^2 = 0.71$; Figures 7b and 7e), and the bias was also seen in the diel

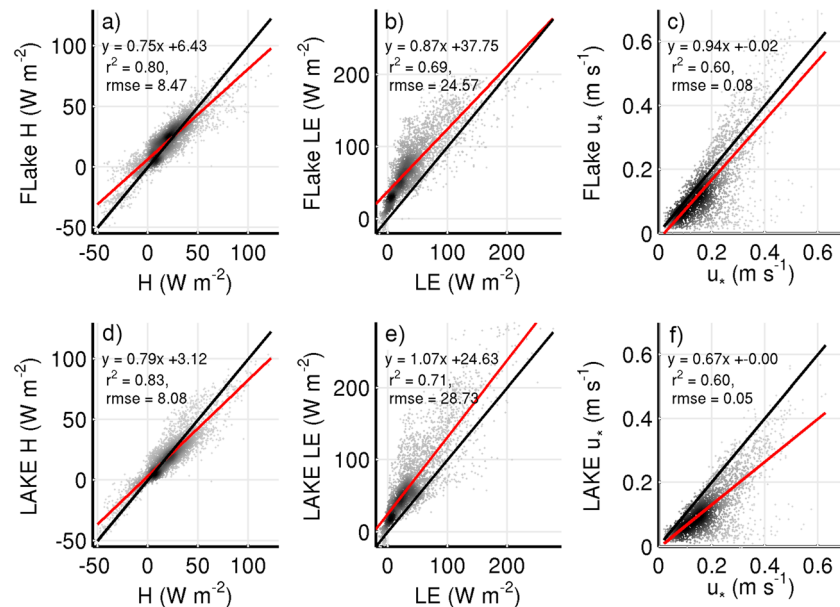


Figure 7. For FLake model, the measured (x axis) versus modeled (y axis) (a) sensible heat flux, (b) latent heat flux, and (c) friction velocity and the (d–f) respective plots for LAKE model. A linear fit (red line) and its coefficients are shown on the subplots, in addition to a 1:1 line (black). The density of data points is shown with shades of gray (arbitrary units, i.e., points/area).

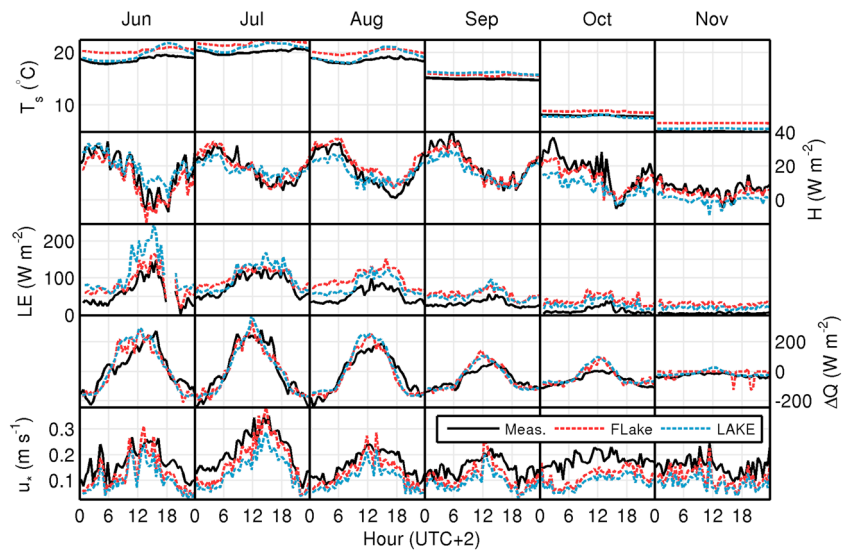


Figure 8. Diel course averaged over 1 month of surface temperature (T_s), sensible heat flux (H), latent heat flux (LE), heat storage change (ΔQ), and friction velocity (u_*). The measurements (black continuous line), FLake model (red dashed line), and LAKE model (blue dashed line) are shown.

variation. There was a difference between the model runs and measurements of LE which appeared about the same time with the heavy rain event in mid-August. Either the models are unable to capture this or there is some undetected error in the measurements after the event.

Martynov *et al.* [2010] observed that FLake modeled LE reasonably well but H was overestimated up to 50%. In Thiery *et al.* [2014a], FLake gave higher estimates than LAKE for both LE and H . However, they concluded that FLake was very sensitive to model configuration in their study of a deep, tropical lake. In our study, since the measured and modeled H were in agreement even though the modeled T_s was about 1°C too high, probably too much of the available energy was allocated to LE . Inaccuracies in humidity data could affect LE , but we believe that there was no significant bias in the forcing data. Another reason for the bias could be the inaccuracy of the calculated heat storage change in the water body, but this is unlikely since the resistance thermometers used are precise and the modeled and calculated change in heat storage were in agreement. However, some bias may have been produced by using spot samples of temperature (thermistor string) to represent the temperatures of an area (EC footprint). Furthermore, the friction velocity was underestimated by both models (Figures 7c and 7e and Figure 8), despite the increased Charnock number (see section 3.2).

3.5. Model Sensitivity to Water Clarity

To compare our results to other existing studies, K_d was varied 25% around its true value. The seasonal average of surface water and epilimnion were colder by 0.31°C and 0.63°C (FLake) and 0.32°C and 0.68°C (LAKE), respectively, when the water was darker. Perroud and Goyette [2010] simulated the water temperature profile of Lake Geneva (Switzerland, 580 km²) using the SIMSTRAT 1-D lake model and varied K_d (estimated from Secchi depth) by $\pm 25\%$. They showed that the maximum monthly difference between the two simulations in the epilimnetic temperature was 0.33°C. Read and Rose [2013] simulated the water temperature profile of Trout Bog (Wisconsin, USA; 0.015 km², $K_d = 3.51 \text{ m}^{-1}$) with a mechanistic model and varied the DOC concentration by $\pm 50\%$. This was equivalent to 11% change in K_d (according to their Figure 1). They showed that the water temperatures were $>2^\circ\text{C}$ lower in the dark-water case than in the clear-water simulation.

When K_d increases, more energy is absorbed in near-surface water which leads to higher surface temperatures and increased H and LE . When K_d was increased by 25%, both turbulent fluxes increased: H by 3.4% (FLake) and 1.6% (LAKE) and LE by 4.0% and 2.3%, respectively. Potes *et al.* [2012] studied Alqueva Reservoir (Portugal; 250 km², eutrophic) using FLake with two extreme values of K_d (1.0 m^{-1} and 6.1 m^{-1}). They concluded that the simulated diel range of surface temperature increased by 1.2°C and the sensible

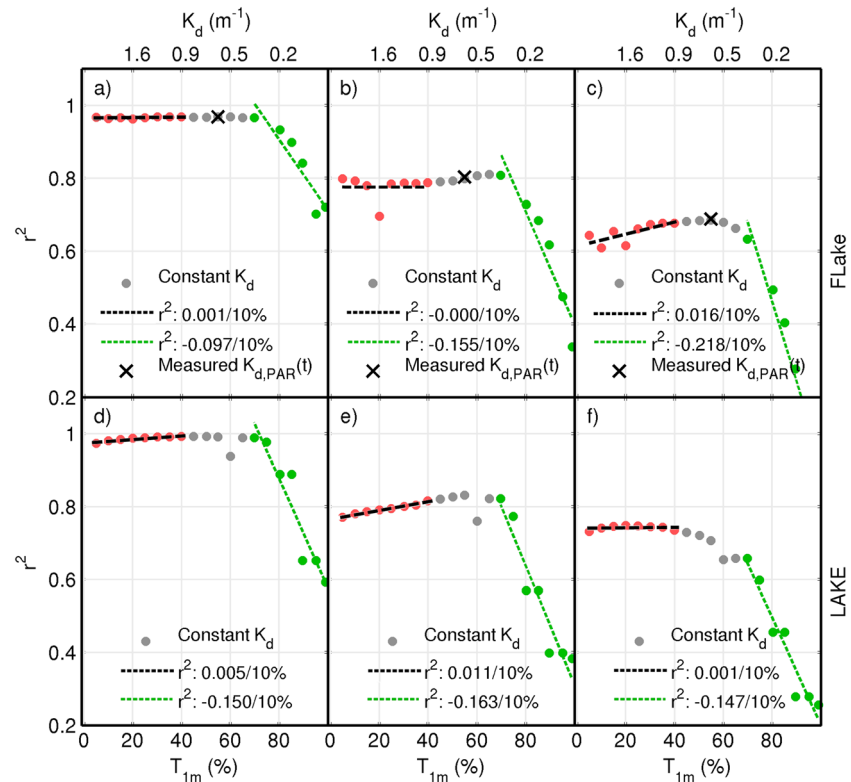


Figure 9. For FLake model, the correlations (y axis) between measured and modeled (a) surface temperature, (b) sensible heat flux, and (c) latent heat flux and the (d–f) respective correlations for LAKE model. The x axis is given in terms of the extinction coefficient (K_d , top) and percent transmission per meter (T_{1m} , bottom). Each of the dots represent one run with fixed K_d , and the red color denotes the simulations with darker water and green with clearer water (see also linear fits in panels), and the black crosses denote the experiments with the measured time-evolving K_d (only for FLake).

and latent heat fluxes increased by 7% and 3%, respectively. In this study, H and LE increased by 8% and 5% (FLake) when K_d was increased from 1 m^{-1} to 3 m^{-1} .

Correlations between the measured and simulated surface temperature and turbulent fluxes were best when a realistic K_d was used (gray circles in Figure 9). When simulations were done with too high T_{1m} (i.e., low K_d), the coefficient of determination between the simulated and measured fluxes decreased fast, by about 0.15 per 10% change in T_{1m} . Contrastingly, the sensitivity to a too low T_{1m} (high K_d) was negligible since the optical depth was much less than the mixing depth. When K_d is estimated to be lower than measured, a rapid increase in the amount of radiation penetrating below the epilimnion is observed, whereas in the case of too high estimate of K_d , the change in penetrating radiation is much smaller [see Hocking and Straškraba, 1999] (Figure 3). We found the critical threshold for K_d to be $\sim 0.5\text{ m}^{-1}$, which supported the results by Rinke *et al.* [2010]. Thus, the response of 1-D lake models is nonlinear with respect to K_d , and the models are much more sensitive if the water is estimated to be too clear.

With FLake, an additional simulation (black crosses in Figure 9) was made with 21 day running median-filtered values of the measured K_{dPAR} (Figure 4). In Lake Kuivajärvi, the simulation with a constant K_d value (observed average over the study period) and a time-dependent value produced very similar results (Student’s t test, $P=0.01$). There was no observable seasonal difference either, and turbulent fluxes were not significantly affected.

3.6. Differences in Stratification Patterns in Clear- and Dark-Water Simulations

The two models were run with 20 logarithmically evenly spaced K_d values ($0.01\text{--}3.00\text{ m}^{-1}$) that were kept constant throughout the simulation period. However, the results of LAKE are discussed here since it represented the thermal behavior of Lake Kuivajärvi more precisely.

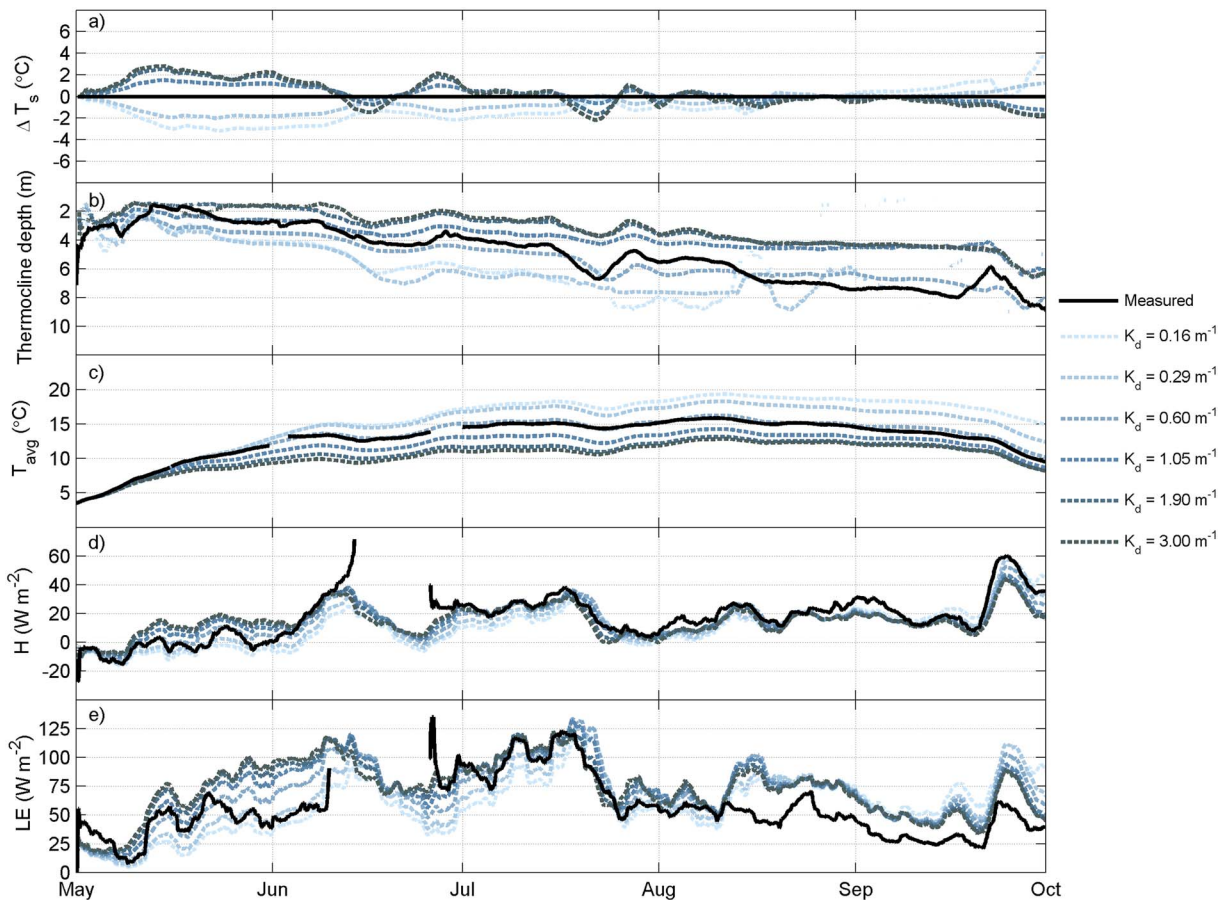


Figure 10. Time series (5 day running mean) of (a) surface water temperature gradient between model runs with measured and fixed K_d , (b) thermocline depth, (c) average water column temperature, and (d) sensible and (e) latent heat fluxes. The measured value (thick black line) in addition to the values from selected LAKE model runs with fixed light extinction coefficient values (K_d , legend) in 2013 before autumn turnover are shown. For figure clarity, only a selection of runs is presented.

Clear water allows the light to penetrate deep into the water. The resulting heat energy is distributed to a larger volume leading to lower surface water temperatures, T_s (Figure 10a), and deeper thermocline formation (Figure 10b). After the beginning, when the thermocline had developed at about the same depth (2 m) in all 20 simulations, the deepening was much faster for simulations with a low K_d . The sign of surface water temperature response to smaller K_d changed from negative to positive roughly when summer stratification period was superseded by autumnal mixing (Figure 10a). During summer stratification, T_s was higher for larger K_d values due to larger fraction of solar radiation absorbed in the mixed layer. However, mean water column temperature, T_{avg} , was lower (Figure 10c) due to enhanced heat loss at the surface via longwave radiation and sensible and latent heat fluxes (Figures 10d and 10e). As a result, by beginning of fall overturn, lake with smaller K_d has accumulated more heat, and during overturn the surface temperature is higher than in a lake with higher K_d . Due to differences in heat loss, in our study when the maximum T_{avg} was reached in August, it was about 10°C lower in the darkest water simulation ($K_d=3.0\text{ m}^{-1}$) as opposed to the clearest water run ($K_d=0.01\text{ m}^{-1}$). *Hocking and Straškraba* [1999] carried out similar modeling with same kind of findings on the effect of changes in K_d on T_s , T_{avg} , and thermocline depth. Also, the surface water temperature response to K_d changed sign at the onset of autumn overturn (their Figure 9a). *Jones et al.* [2005] observed constantly higher T_s and lower T_{avg} in a closure with high Chl *a* compared to low Chl *a* closure. Unfortunately, they had no optical measurements, and therefore, these results cannot be related to K_d values.

According to simulations with different, fixed K_d , the seasonal thermal progress of the lake depended nonlinearly on K_d . During spring the lake heated at different rates depending on K_d . However, during the period from mid-July to the end of August, the surface water temperature was very similar (i.e., $\Delta T_s < \pm 2^\circ\text{C}$) in almost all the model runs (Figure 10a), which resulted in similar cooling rates in the end of summer. These

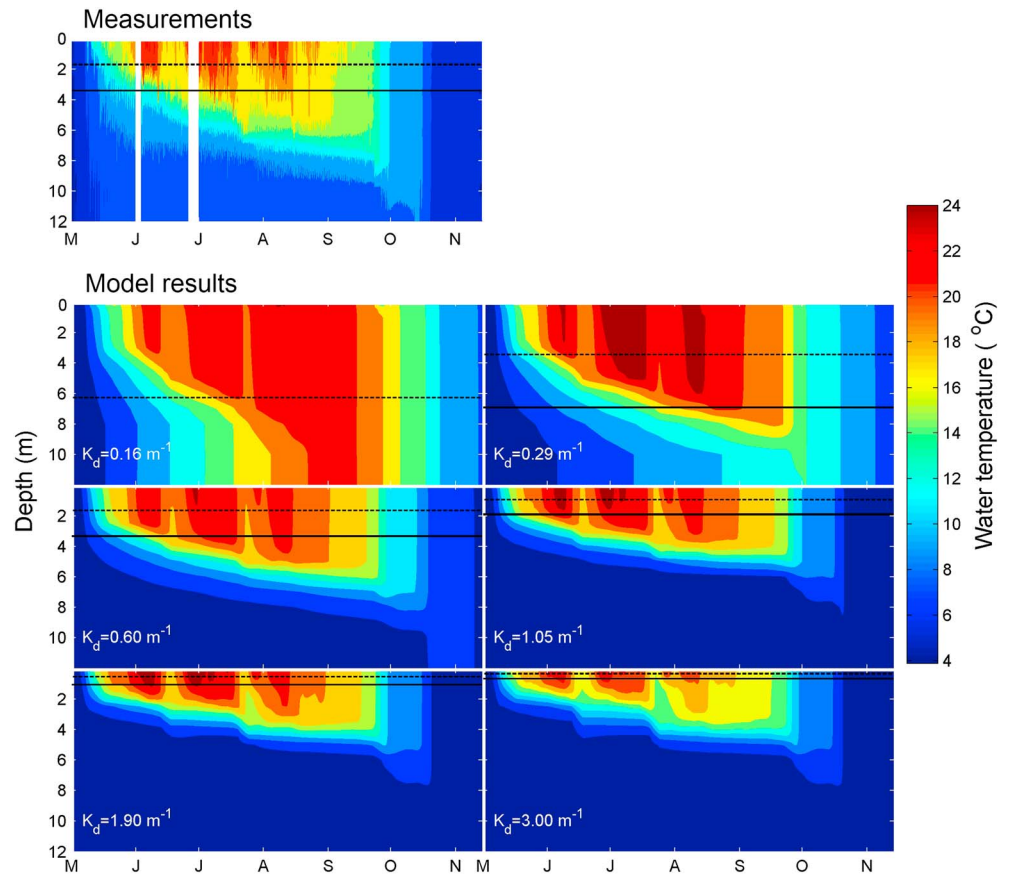


Figure 11. The isotherms of Lake Kuivajärvi throughout the open-water period 2013. The top left are the measured temperatures, and the others are modeled with LAKE using fixed K_d . The horizontal dashed black line represents the optical depth (K_d^{-1}) and the solid black line the euphotic depth ($2 \times K_d^{-1}$).

resulted in much higher T_{avg} in clear-water simulations (16°C) as opposed to the dark-water ones (8°C) at the time of the onset of autumn overturn. Before the autumn overturn, there was a 4 m difference in the thermocline depth between the simulation with clearest and darkest water. Rinke *et al.* [2010] compared the simulated temperature difference between the surface and 20 m depth and noticed that in dark-water simulations, the surface water both heated and cooled more rapidly, so that a cooling phase following a heating phase can quickly destroy the differences in thermal stratifications between runs with different K_d (their Figure 6). Our results seem to indicate that heating and cooling are not equal and opposing processes in lakes since heating occurs over a wide depth range (typically extending meters below the surface) and cooling only over the thin air-water interface. Therefore, in our study, cooling did not completely counteract the effect of heating on the thermal structure of the lake between simulations with different K_d .

In general, the darker water runs had an earlier and stronger onset of stratification, mixed layer was shallower, and autumn overturn began earlier with lower water column temperatures (Figure 11). Since the heat content of dark-water lake is lower after the onset of autumn overturn, the surface water is more prone to reach freezing temperatures. This distinction between clear- and dark-water lake is more pronounced the earlier the winter starts during the particular year. If the onset of the winter is prolonged, there is more time for the clear-water lake to lose heat and “catch up” the dark-water lake. Therefore, this could suggest that as a whole the open-water period is actually shortened if the water becomes more turbid.

In Lake Kuivajärvi, model runs with low K_d showed that the mixed layer is shallower than the euphotic zone; i.e., primary producers always stay in the euphotic layer. However, it seems that the euphotic layer depth is decreased faster than the mixed layer depth when K_d is increased, so that in dark water the primary producers can be transported to depths where there is insufficient light for primary production. For example,

with $K_d = 0.6 \text{ m}^{-1}$, the euphotic depth was almost always below the mixed layer until mid-August, whereas with $K_d = 1.05 \text{ m}^{-1}$, the mixed layer was deeper than euphotic depth most of the time already after June (Figure 11).

The stronger thermocline due to higher K_d could inhibit the mixing of hypolimnetic waters to the epilimnion and hinder the entrainment of nutrients, as discussed in Jones *et al.* [2005]. On the other hand, Hocking *et al.* [1999] noticed that since the epilimnion is shallower when K_d is higher, less energy is needed to mix the shallow warmer layer and therefore more energy is available for further deepening of the mixed layer. Note that mixed layer and thermocline depth are not equivalent measures but in the case of strong mixing and sharp thermocline they can have more or less equal values, as is typical of Lake Kuivajärvi. Our data seem to lend support to the finding by Hocking *et al.* [1999], since after the strong wind event in mid-July, the thermocline deepened the most in dark-water simulations and least in clear-water ones. It has been estimated for Lake Kuivajärvi that high concentrations of CO_2 can be upwelled from hypolimnetic waters during strong winds [Heiskanen *et al.*, 2014], but it is uncertain whether increase in K_d would decrease the entrainment of nutrients or would it actually be increased, because nutrient dynamics were not incorporated to the models in the current study.

4. Summary and Conclusions

Simulations of lake-atmosphere interaction and lake thermal regime were done using two 1-D lake models (FLake and LAKE), and results were compared with direct measurements from Lake Kuivajärvi (area 0.62 km^2 , median $K_d = 0.59 \text{ m}^{-1}$). The observational data set is composed of EC fluxes, a lake water temperature profile, and water clarity measurements in addition to basic meteorological variables. Simulations were performed for 20 different water clarities, and an additional simulation with FLake was done using 30 min averaged measured K_d as a driving variable.

Both lake models were very sensitive to K_d if simulations were performed with too low values (clearer than actual water). In this case, the coefficient of determination between the simulated and measured turbulent fluxes decreased fast, by about 0.15 per 10% change in $T_{1 \text{ m}}$. In contrast, the sensitivity to higher than actual K_d was negligible. Thus, we recommend that if the clarity of a lake is not known exactly, it is better to use a value of K_d that is too high than too low in lake simulations. We believe that NWP in regions of relatively clear lakes (e.g., at high altitudes) will benefit most from a global mapping of K_d . Such a global map could be created using satellite remote sensing, as was done for Lake Taihu [Wang *et al.*, 2011] and Alqueva reservoir [Potes *et al.*, 2012]. The simulations with the FLake model were not improved when time-dependent K_d was applied as opposed to using a fixed K_d (average measured K_d over the whole open-water period). Therefore, it is adequate to start a time-independent global mapping of K_d for future use in NWP.

The roughness length in model parameterizations was substantially increased (Charnock $\alpha = 0.38$), but the friction velocity was still underestimated by both models. In the simulations with a seasonally averaged K_d , surface water temperature was overestimated by about 1°C by both models, but the diel and seasonal variations of the change in heat storage were adequately simulated. Sensible heat was simulated without a bias, but seasonally averaged latent heat flux was overestimated by both models by over 30%. In general, both models described the lake-atmosphere interaction satisfyingly. Although it was outside the scope of this work, it is evident that more attention should be given to the roughness parameterizations in small sheltered lakes.

According to our model runs, during summer the mixed layer depth is smaller than the euphotic depth when K_d is $< 0.6 \text{ m}^{-1}$. Therefore, in small lakes with low winds and shallow mixed layers, the primary producers typically reside in the euphotic layer. Darker water could, however, lead to light limitation of primary production since the euphotic depth seems to decrease faster than the mixed layer depth.

We observed that changes in K_d had nonlinear effects on the thermal stratification when the models were run with different, fixed K_d . While the progress of the stratification differed between these runs during the spring, the autumnal decay occurred at the same rate, leading to much lower water column temperatures during the autumn overturn when K_d was high. This could lead to earlier ice cover in dark-water lakes since the lake heat content is lower in late autumn. Thus, climate change-related alterations in precipitation patterns and resulting changes in CDOM loading could lead to very different thermal stratification and alter the onset of ice cover, both of which would have significant impact on lake-biota and lake-atmosphere interactions.

Acknowledgments

The study was supported by EU projects InGOS, GHG-LAKE (project 612642), ICOS-ERIC (281250), Nordic Centre of Excellence DEFROST, Academy of Finland (National Centre of Excellence (272041), ICOS (projects 271878 and 281255), PACE, CarLAC (281196) and China project) and project 256082 (Flux measurements of greenhouse gases for agricultural, lake, and wetland ecosystems and process modeling of wetland methane production). M.L. was supported by the Nordic Centre of Excellence programme CRAICC and AO by the Academy of Finland (project 139291). A.N. thanks Väisälä foundation for its support. V.S. is indebted to Russian Foundation for Basic Research (grant 14-05-91752). The data are available from the author upon request (jouni.heiskanen@helsinki.fi).

References

- Arst, H., S. Mäekivi, and T. Lukk (1997), Calculating irradiance penetration into water bodies from the measured beam attenuation coefficient, *Limnol. Oceanogr.*, *42*(2), 379–385.
- Arst, H., A. Erm, A. Herlevi, T. Kutser, M. Leppäranta, A. Reinart, and J. Virta (2008), Optical properties of boreal lake waters in Finland and Estonia, *Boreal Environ. Res.*, *13*, 133–158.
- Balsamo, G., R. Salgado, E. Dutra, S. Boussetta, T. Stockdale, and M. Potes (2012), On the contribution of lakes in predicting near-surface temperature in a global weather forecasting model, *Tellus A*, *64*, 1–12, doi:10.3402/tellusa.v64i0.15829.
- Charnock, H. (1955), Wind stress on a water surface, *Q. J. R. Meteorol. Soc.*, *81*(350), 639–640, doi:10.1002/qj.49708135026.
- Chechin, D. G., I. A. Repina, and V. M. Stepanenko (2010), Numerical modeling of the influence of cool skin on the heat balance and thermal regime of a water body, *Izv. Atmos. Oceanic Phys.*, *46*(4), 499–510, doi:10.1134/S0001433810040092.
- Clement, R. J. (2004), Mass and energy exchange of a plantation forest in Scotland using micrometeorological methods, chap. 5, PhD dissertation, Univ. of Edinburgh, U. K.
- Cole, J. J., et al. (2007), Plumbing the global carbon cycle: Integrating inland waters into the terrestrial carbon budget, *Ecosystems*, *10*(1), 172–184, doi:10.1007/s10021-006-9013-8.
- Downing, J. A. (2010), Emerging global role of small lakes and ponds: Little things mean a lot, *Limnetica*, *29*(1), 9–23.
- Dutra, E., V. M. Stepanenko, G. Balsamo, P. Viterbo, P. M. A. Miranda, D. Mironov, and C. Schär (2010), An offline study of the impact of lakes on the performance of the ECMWF surface scheme, *Boreal Environ. Res.*, *15*, 100–112.
- Eerola, K., L. Rontu, E. Kourzeneva, and E. Shcherbak (2010), A study on effects of lake temperature and ice cover in HIRLAM, *Boreal Environ. Res.*, *15*, 130–142.
- Fee, E. J., R. E. Hecky, S. E. M. Kasian, and D. R. Cruikshank (1996), Physical and chemical responses of lakes and streams, *Limnol. Oceanogr.*, *41*(5), 912–920.
- Findlay, S. E. G., and R. L. Sinsabaugh (2003), *Aquatic Ecosystems: Interactivity of Dissolved Organic Matter*, Elsevier Academic Press, San Diego, Calif.
- Foken, T., and B. Wichura (1996), Tools for quality assessment of surface-based flux measurements, *Agric. For. Meteorol.*, *78*, 83–105, doi:10.1016/0168-1923(95)02248-1.
- Gaiser, E. E., N. D. Deyrup, R. W. Bachmann, L. E. Battoe, and H. M. Swain (2009), Multidecadal climate oscillations detected in a transparency record from a subtropical Florida lake, *Limnol. Oceanogr.*, *54*(6), 2228–2232.
- Hari, P., and M. Kulmala (2005), Station for Measuring Ecosystem–Atmosphere Relations (SMEAR II), *Boreal Environ. Res.*, *10*, 315–322.
- Heiskanen, J. J., I. Mammarella, S. Haapanala, J. Pumpanen, T. Vesala, S. MacIntyre, and A. Ojala (2014), Effects of cooling and internal wave motions on gas transfer coefficients in a boreal lake, *Tellus B*, *66*, 1–16, doi:10.3402/tellusb.v66.22827.
- Hieronymi, M., and A. Macke (2012), On the influence of wind and waves on underwater irradiance fluctuations, *Ocean Sci.*, *8*, 455–471, doi:10.5194/os-8-455-2012.
- Hocking, G. C., and M. Straškraba (1999), The effect of light extinction on thermal stratification in reservoirs and lakes, *Int. Rev. Hydrobiol.*, *84*, 535–556.
- Jeppesen, E., J. P. Jensen, M. Søndergaard, and T. Lauridsen (1999), Trophic dynamics in turbid and clearwater lakes with special emphasis on the role of zooplankton for water clarity, *Hydrobiologia*, *408*(409), 217–231.
- Ji, Z.-G. (2008), *Hydrodynamics and Water Quality: Modeling Rivers, Lakes, and Estuaries*, 1st ed., John Wiley, Hoboken, N. J.
- Jones, I., G. George, and C. Reynolds (2005), Quantifying effects of phytoplankton on the heat budgets of two large limnetic enclosures, *Freshwater Biol.*, *50*, 1239–1247.
- Kaimal, J. C., and J. J. Finnigan (1994), *Atmospheric Boundary Layer Flows, Their Structure and Measurements*, Oxford Univ. Press, New York.
- Kirillin, G. (2010), Modeling the impact of global warming on water temperature and seasonal mixing regimes in small temperate lakes, *Boreal Environ. Res.*, *15*, 279–293.
- Kirillin, G., J. Hochschild, D. Mironov, A. Terzhevik, S. Golosov, and G. Nützmann (2011), FLake-Global: Online lake model with worldwide coverage, *Environ. Modell. Software*, *26*(5), 683–684, doi:10.1016/j.envsoft.2010.12.004.
- Kirk, J. T. O. (2011), *Light and Photosynthesis in Aquatic Ecosystems*, 3rd ed., Cambridge Univ. Press, Cambridge, U. K.
- Kourzeneva, E., E. Martin, Y. Batrak, and P. Le Moigne (2012), Climate data for parameterisation of lakes in numerical weather prediction models, *Tellus A*, *64*, 1–17, doi:10.3402/tellusa.v64i0.17226.
- Lei, R., M. Leppäranta, A. Erm, E. Jaatinen, and O. Pärn (2011), Field investigations of apparent optical properties of ice cover in Finnish and Estonian lakes in winter 2009, *Est. J. Earth Sci.*, *60*(1), 50–64, doi:10.3176/earth.2011.1.05.
- Leppäranta, M. (2015), *Freezing of Lakes and the Evolution of Their Ice Cover*, Springer-Praxis, Heidelberg, Germany.
- Liu, H., G. Peters, and T. Foken (2001), New equations for sonic temperature variance and buoyancy heat flux with an omnidirectional sonic anemometer, *Boundary Layer Meteorol.*, *100*, 459–468.
- Mammarella, I., S. Launiainen, T. Gronholm, P. Keronen, J. Pumpanen, Ü. Rannik, and T. Vesala (2009), Relative humidity effect on the high-frequency attenuation of water vapor flux measured by a closed-path eddy covariance system, *J. Atmos. Oceanic Technol.*, *26*(9), 1856–1866, doi:10.1175/2009JTECHA1179.1.
- Mammarella, I., et al. (2015), Carbon dioxide and energy fluxes over a small boreal lake in southern Finland, *J. Geophys. Res. Biogeosci.*, *120*, doi:10.1002/2014JG002873.
- Martynov, A., L. Sushama, and R. Laprise (2010), Simulation of temperate freezing lakes by one-dimensional lake models: Performance assessment for interactive coupling with regional climate models, *Boreal Environ. Res.*, *15*, 143–164.
- Miettinen, H., J. Pumpanen, J. J. Heiskanen, H. Aaltonen, I. Mammarella, A. Ojala, J. Levula, and M. Rantakari (2015), Towards a more comprehensive understanding of lacustrine greenhouse gas dynamics—Two-year measurements of concentrations and fluxes of CO₂, CH₄ and N₂O in a typical boreal lake surrounded by managed forests, *Boreal Environ. Res.*, *20*, 75–89.
- Mironov, D., E. Heise, E. Kourzeneva, B. Ritter, N. Schneider, and A. Terzhevik (2010), Implementation of the lake parameterisation scheme FLake into the numerical weather prediction model COSMO, *Boreal Environ. Res.*, *15*, 218–230.
- Morris, D. P., H. Zagarese, C. E. Williamson, E. G. Balseiro, B. R. Hargreaves, B. Modenutti, R. Moeller, and C. Queimalinos (1995), The attenuation of solar UV radiation in lakes and the role of dissolved organic carbon, *Limnol. Oceanogr.*, *40*, 1381–1391, doi:10.4319/lo.1995.40.8.1381.
- Niemistö, J. (2008), Sediment resuspension as a water quality regulator in lakes Doctoral dissertation, Dep. Biol. and Environ., Univ. of Helsinki, Helsinki Univ. Print, Helsinki, Finland.
- Niiler, P. P., and E. B. Kraus (1977), One-dimensional models of the upper ocean, in *Modelling and Prediction of the Upper Layers of the Ocean*, edited by E. B. Kraus, pp. 143–172, Pergamon Press, Oxford, U. K.
- Nordbo, A., S. Launiainen, I. Mammarella, M. Leppäranta, J. Huotari, A. Ojala, and T. Vesala (2011), Long-term energy flux measurements and energy balance over a small boreal lake using eddy covariance technique, *J. Geophys. Res.*, *116*, D02119, doi:10.1029/2010JD014542.

- Nordbo, A., L. Järvi, and T. Vesala (2012), Revised eddy covariance flux calculation methodologies—Effect on urban energy balance, *Tellus B*, *64*, 1–20, doi:10.3402/tellusb.v64i0.18184.
- Ojala, A., J. López Bellido, T. Tulonen, P. Kankaala, and J. Huotari (2011), Carbon gas fluxes from a brown-water and a clear-water lake in the boreal zone during a summer with extreme rain events, *Limnol. Oceanogr.*, *56*, 61–76, doi:10.4319/lo.2011.56.01.0061.
- Pace, M. L., and J. J. Cole (2002), Synchronous variation of dissolved organic carbon and color in lakes, *Limnol. Oceanogr.*, *47*, 333–342.
- Perroud, M., and S. Goyette (2010), Impact of warmer climate on Lake Geneva water-temperature profiles, *Boreal Environ. Res.*, *15*, 255–278.
- Persson, I., and I. D. Jones (2008), The effect of water colour on lake hydrodynamics: A modelling study, *Freshwater Biol.*, *53*, 2345–2355, doi:10.1111/j.1365-2427.2008.02049.x.
- Potes, M., M. J. Costa, and R. Salgado (2012), Satellite remote sensing of water turbidity in Alqueva reservoir and implications on lake modelling, *Hydrol. Earth Syst. Sci.*, *16*, 1623–1633, doi:10.5194/hess-16-1623-2012.
- Rae, R., C. Howard-Williams, I. Hawes, A.-M. Schwarz, and W. F. Vincent (2001), Penetration of solar ultraviolet radiation into New Zealand lakes: Influence of dissolved organic carbon and catchment vegetation, *Limnology*, *2*, 79–89.
- Read, J. S., and K. C. Rose (2013), Physical responses of small temperate lakes to variation in dissolved organic carbon concentrations, *Limnol. Oceanogr.*, *58*, 921–931, doi:10.4319/lo.2013.58.3.0921.
- Rinke, K., P. Yeates, and K.-O. Rothhaupt (2010), A simulation study of the feedback of phytoplankton on thermal structure via light extinction, *Freshwater Biol.*, *55*, 1674–1693.
- Rontu, L., K. Eerola, E. Kourzeneva, and B. Vehviläinen (2012), Data assimilation and parameterisation of lakes in HIRLAM, *Tellus A*, *64*, 1–12, doi:10.3402/tellusa.v64i0.17611.
- Rooney, G. G., and F. J. Bornemann (2013), The performance of FLake in the Met Office Unified Model, *Tellus A*, *65*, 1–16, doi:10.3402/tellusa.v65i0.21363.
- Rooney, G. G., and I. D. Jones (2010), Coupling the 1-D lake model FLake to the community land-surface model JULES, *Boreal Environ. Res.*, *15*, 501–512.
- Salgado, R., and P. Le Moigne (2010), Coupling of the FLake model to the Surfex externalized surface model, *Boreal Environ. Res.*, *15*, 231–244.
- Schulz, S., H. Matsuyama, and R. Conrad (1997), Temperature dependence of methane production from different precursors in a profundal sediment (Lake Constance), *FEMS Microbiol. Ecol.*, *22*, 207–213.
- Stepanenko, V. M., E. E. Machul'skaya, M. V. Glagolev, and V. N. Lykossov (2011), Numerical modeling of methane emissions from lakes in the permafrost zone, *Izv. Atmos. Oceanic Phys.*, *47*, 252–264, doi:10.1134/S0001433811020113.
- Stepanenko, V. M., A. Martynov, K. D. Jöhnk, Z. M. Subin, M. Perroud, X. Fang, F. Beyrich, D. Mironov, and S. Goyette (2013), A one-dimensional model intercomparison study of thermal regime of a shallow, turbid midlatitude lake, *Geosci. Model Dev.*, *6*, 1337–1352, doi:10.5194/gmd-6-1337-2013.
- Stepanenko, V., K. D. Jöhnk, E. Machul'skaya, M. Perroud, Z. Subin, A. Nordbo, I. Mammarella, and D. Mironov (2014), Simulation of surface energy fluxes and stratification of a small boreal lake by a set of one-dimensional models, *Tellus A*, *66*, 1–18, doi:10.3402/tellusa.v66.21389.
- Subin, Z. M., W. J. Riley, and D. Mironov (2012), An improved lake model for climate simulations: Model structure, evaluation, and sensitivity analyses in CESM1, *J. Adv. Model. Earth Syst.*, *4*, M02001, doi:10.1029/2011MS000072.
- Thiery, W., et al. (2014a), LakeMIP Kivu: Evaluating the representation of a large, deep tropical lake by a set of one-dimensional lake models, *Tellus A*, *66*, 1–18, doi:10.3402/tellusa.v66.21390.
- Thiery, W., A. Martynov, F. Darchambeau, J.-P. Descy, P.-D. Plisnier, L. Sushama, and N. P. M. van Lipzig (2014b), Understanding the performance of the FLake model over two African Great Lakes, *Geosci. Model Dev.*, *7*, 317–337.
- Tranvik, L. J., et al. (2009), Lakes and reservoirs as regulators of carbon cycling and climate, *Limnol. Oceanogr.*, *54*(6, part 2), 2298–2314.
- Ventelä, A.-M., M. Tarvainen, H. Helminen, and J. Sarvala (2007), Long-term management of Pyhäjärvi (southwest Finland): Eutrophication, restoration—Recovery?, *Lake Reservoir Manage.*, *23*, 428–438, doi:10.1080/07438140709354028.
- Vesala, T., W. Eugster, and A. Ojala (2012), Eddy covariance measurements over lakes, in *Eddy Covariance: A Practical Guide to Measurement and Data Analysis*, edited by M. Aubinet, T. Vesala, and D. Papale, Springer, Dordrecht, Netherlands.
- Vickers, D., and L. Mahrt (1997a), Fetch limited drag coefficients, *Boundary-Layer Meteorol.*, *85*, 53–79.
- Vickers, D., and L. Mahrt (1997b), Quality control and flux sampling problems for tower and aircraft data, *J. Atmos. Oceanic Technol.*, *14*, 512–526.
- Wang, M., W. Shi, and J. Tang (2011), Water property monitoring and assessment for China's inland Lake Taihu from MODIS-Aqua measurements, *Remote Sens. Environ.*, *115*, 841–854, doi:10.1016/j.rse.2010.11.012.
- Weyhenmeyer, G. A. (1998), Resuspension in lakes and its ecological impact—A review, *Arch. Hydrobiol. Spec. Issues Adv. Limnol.*, *51*, 185–200.
- White, B., J. Austin, and K. Matsumoto (2012), A three-dimensional model of Lake Superior with ice and biogeochemistry, *J. Great Lakes Res.*, *38*, 61–71, doi:10.1016/j.jglr.2011.12.006.
- Wik, M., B. F. Thornton, D. Bastviken, S. Macintyre, R. K. Varner, and P. M. Crill (2014), Energy input is primary controller of methane bubbling in subarctic lakes, *Geophys. Res. Lett.*, *14*, 1–6, doi:10.1002/2013GL058510.
- Williamson, C. E., R. S. Stemberger, D. P. Morris, T. A. I. Frost, and S. G. Paulsen (1996), Ultraviolet radiation in North American lakes: Attenuation estimates from DOC measurements and implications for plankton communities, *Limnol. Oceanogr.*, *41*, 1024–1034.
- Wüest, A., and A. Lorke (2003), Small-scale hydrodynamics in lakes, *Annu. Rev. Fluid Mech.*, *35*, 373–412, doi:10.1146/annurev.fluid.35.101101.161220.
- Yang, Y., B. Cheng, E. Kourzeneva, T. Semmler, L. Rontu, M. Leppäranta, K. Shirasawa, and Z. Li (2013), Modelling experiments on air–snow–ice interactions over Kilpisjärvi, a lake in northern Finland, *Boreal Environ. Res.*, *18*, 341–358.
- Zheng, X., T. Dickey, and G. Chang (2002), Variability of the downwelling diffuse attenuation coefficient with consideration of inelastic scattering, *Appl. Opt.*, *41*, 6477–88.